

Asymmetric Evolution of Magnetic Reconnection in Collisionless Accretion Disk

Keisuke Shirakawa^{1, a)} and Masahiro Hoshino¹

Department of Earth and Planetary Science, The University of Tokyo, 7-3-1 Hongo, Bunkyo-ku, Tokyo, Japan

(Dated: 28 May 2022)

An evolution of a magnetic reconnection in a collisionless accretion disk is investigated using a 2.5 dimensional hybrid code simulation. In astrophysical disks magnetorotational instability (MRI) is considered to play an important role by generating turbulence in the disk and contributes to an effective angular momentum transport through a turbulent viscosity. Magnetic reconnection, on the other hand also plays an important role on the evolution of the disk through a dissipation of a magnetic field enhanced by a dynamo effect of MRI. In this study, we developed a hybrid code to calculate an evolution of a differentially rotating system. With this code, we first confirmed a linear growth of MRI. We also investigated a behavior of a particular structure of a current sheet which would exist in the turbulence in the disk. From the calculation of the magnetic reconnection, we found an asymmetric structure in the out-of-plane magnetic field during the evolution of reconnection which can be understood by a coupling of the Hall effect and the differential rotation. We also found a migration of X-point whose direction is determined only by an initial sign of $\mathbf{J}_0 \times \boldsymbol{\Omega}_0$ where \mathbf{J}_0 is the initial current density in the neutral sheet and $\boldsymbol{\Omega}_0$ is the rotational vector of the background Keplerian rotation. Associated with the migration of X-point we also found a significant enhancement of the perpendicular magnetic field compared to an ordinary MRI. MRI-Magnetic reconnection coupling and the resulting magnetic field enhancement can be an effective process to sustain a strong turbulence in the accretion disk and to a transport of angular momentum.

Keywords: Magnetic Reconnection, Accretion Disk, Magneto Rotational Instability, Collisionless Plasma

I. INTRODUCTION

Transport of angular momentum in accretion disks has been one of the fundamental problems in astrophysics. For the efficient transport of the angular momentum, turbulence generated in a disk is believed to play an important role through strong turbulent viscosity [Shakura and Sunyaev (1973)]. The most promising process to generate turbulence in accretion disks is the magnetorotational instability (MRI) which is driven by a strong dynamo effect of a shear flow provided by the differential rotation of the disk [Velikhov (1959); Chandrasekhar (1960); Balbus and Hawley (1991)]. Since the turbulence in the disk determines the efficiency of the angular momentum transport, saturation of the MRI has been one of the most important problems. In the saturated, quasi steady state, the dynamo effect of the MRI and some sort of magnetic dissipation must be balanced [Balbus and Hawley (1998)]. Numerous simulation studies have been proposed by many researchers to study the behavior of a quasi steady state of the MRI induced turbulence [Hawley and Balbus (1991); Hawley and Balbus (1992); Matsumoto and Tajima (1995); Sano and Stone (2002)]. During the turbulent state of those calculations rapid amplification and dissipation of magnetic energy have been observed implying magnetic reconnection is playing an important role on the dissipation of magnetic energy.

^{a)}Electronic mail: k-suke@eps.s.u-tokyo.ac.jp

Until now, behavior of the plasma in accretion disks is mainly studied based on a conventional MHD approximation. However, in some classes of accretion disks a mean free path of the plasma is estimated to be comparable to the scale of the disk thickness. For example, several observations suggest that in the accretion disk around Sgr A* at the center of our galaxy the ions and electrons are not in the thermal equilibrium. Since the ions are much hotter than the electrons, the plasma constituting the disk is considered to be collisionless. In such a disk kinetic effect of the plasma is considered to be important since a pressure anisotropy generated by the stretching of the magnetic field modifies a feature of magnetic tension.

Based on these facts, several attempts to understand both linear and nonlinear evolution of collisionless MRI have been made. Quataert, Dorland, and Hammett (2002) have studied a linear behavior of MRI under CGL approximation [Chew, Goldberger, and Low (1956); Kulsrud (1983)] together with parallel heat flux due to the Landau damping incorporated via the so-called Landau closure [Snyder, Hammett, and Dorland (1997)]. They have shown that the pressure anisotropy modifies the linear behavior of the MRI and have suggested that the kinetic plasma effect would also be important in the nonlinear evolution of MRI. Sharma *et al.* (2006) have extended this study to a nonlinear regime by using a so-called collisionless MHD code. Based on the linear analysis, they have applied the CGL approximation together with the Landau closure for calculating the temporal evolution of the parallel and the perpendicular pressure with respect to the local magnetic field. In addition, they have assumed that the upper and the lower limit of the pressure anisotropy is limited by the criteria of the firehose, the mirror and the ion cyclotron instabilities. These instabilities would cause pitch angle scattering of the ions and lead to a relaxation of the generated pressure anisotropy. They have found that with the equation of state based only on the standard CGL approximation, enhancement of the magnetic field generates the perpendicular pressure anisotropy and have obtained a remarkably low saturation level of the MRI. The result was well understood as a suppression of the MRI by the generated perpendicular pressure anisotropy, because the perpendicular pressure anisotropy effectively enhances the magnetic tension which act as the restoring force in the evolution of the MRI. With the parallel heat flux and the appropriate pitch angle scattering model, they confirmed the nonlinear evolution of the MRI and found that the rate of the angular momentum transport is enhanced moderately.

Numerical simulations of MRI capturing full kinetic effects in a consistent manner have been performed by Riquelme *et al.* (2012) and Hoshino (2013) by using a 2.5D PIC code which treats both the ions (the positrons, in Hoshino (2013)) and the electrons as superparticles. Riquelme *et al.* (2012) have shown that during the evolution of the kinetic MRI, the pressure anisotropy has been indeed, relaxed by the mirror mode and have confirmed basic features in the nonlinear stage of the MRI reported in Sharma *et al.* (2006). They have also found that the channel flow and the current sheet which are usually found in the final state of the 2.5D MHD simulations were corrupted due to a magnetic reconnection. Hoshino (2013) has extended the study to a relatively high beta ($\beta \simeq 90-6000$) pair plasma and found the corruption of channel flow as well. Moreover they found that during the “active” phase when the magnetic reconnection takes place repeatedly and the channel flow is corrupted, the Maxwell stress is greatly enhanced. In both simulations particle acceleration associated with the magnetic reconnection has also been observed.

Kinetic effect of plasma is also considered to be important in the evolution of magnetic reconnection. Several *in-situ* observations of the earth’s magnetotail, which is also constituted by a collisionless plasma, have pointed out the existence of thin current sheet [Asano *et al.* (2003)]. In those thin current sheets, the thickness has found to be comparable to the scale of the ion inertia length. In the magnetic reconnection with such a thin current sheet effect of the Hall term in the generalized Ohm’s law is also important [Sonnerup (1979); Terasawa (1983)]. Therefore, for the understanding of the magnetic reconnection in the collisionless accretion disks, the kinetic effect of the plasma, together with the effect of the differential rotation should be taken into account in a self-consistent manner.

For an investigation of kinetic effect of the plasma, PIC simulation gives a self-consistent

picture. However the attainable scale of the method is roughly limited in a several hundred times of the Debye length which is far smaller than that of the actual disk. In addition, as full particle code must resolve a time scale related to the electron physics it requires a massive integration time if one tries to focus both on the Keplerian time scale and on the electron time scale. Moreover, under a “first order” approximation kinetic effect of the ions should be more important than that of the electrons since it is often found in a collisionless accretion disk, the thermal energy of the ions dominates that of the electrons. In this point of view, a hybrid code which treats the ions as particles and the electrons as massless fluid would provide a more robust approach rather than a full particle method.

In this work, we will study an evolution of a differentially rotating system with a hybrid code including the effect of the Coriolis and the tidal force. As a first step, we will mainly focus on an evolution of a magnetic reconnection in the differentially rotating system, which would exist in the turbulence generated by the MRI. The structure of this article is as follows. In Sec. II, we first describe our 2.5D hybrid code which includes the Coriolis and the tidal force with an open shearing boundary condition [Hawley, Gammie, and Balbus (1995)]. Since our simulation here is focused on a 2.5D system, the boundary condition degenerates to a conventional periodic boundary condition for the deviation components from the background differential rotation. Next in Sec. III, we introduce the results of the five consecutive runs. We also briefly introduce the linear growth of the MRI calculated with our hybrid code. At last in Sec. IV, we summarize our results and discuss their effects on the MRI.

II. HYBRID SIMULATION IN A DIFFERENTIALLY ROTATING SYSTEM

We focus on a time evolution of the magnetic reconnection in a localized region of an accretion disk. Under the so-called ‘local approximation’, a number of simulations have been carried out to study a nonlinear evolution of the system under the differential rotation. Those studies which mainly focused on the evolution of the MRI are performed basically under the MHD approximation [Hawley and Balbus (1991); Hawley and Balbus (1992); Matsumoto and Tajima (1995); Sano and Stone (2002)], and recently using PIC codes [Riquelme *et al.* (2012); Hoshino (2013)], taking kinetic plasma effect into account in a self-consistent manner. Basic equations of our simulation are essentially the same with those used in the previous studies, but by using a hybrid code, we took kinetic effect of the ions into account in a self-consistent manner and covered spatially wider region compared to those calculated in PIC simulations. Like in the MHD and the PIC calculations, one must pay attention to the boundary conditions in the differentially rotating system. A brief introduction about the boundary condition is given in Appendix A.

A. Basic Equations

As we focus on a local evolution of the magnetic reconnection, we describe a set of equations in a local corotating frame with the angular velocity of $\boldsymbol{\Omega}_0$ at the distance of r_0 from the central massive object. In this rotating coordinate, we solve a set of Lorentz-Maxwell equations. The ions are treated as superparticles and their motion is calculated with the Lorentz equation including the Coriolis force, the centrifugal force, and gravity, expressed with the cylindrical representation (r, φ, z) ,

$$m_i \frac{d\mathbf{v}_i}{dt} = e \left(\mathbf{E} + \frac{1}{c} \mathbf{v}_i \times \mathbf{B} \right) - 2m_i \boldsymbol{\Omega}_0 \times \mathbf{v}_i + m_i r_i \Omega_0^2 \mathbf{e}_r - m_i g(\mathbf{r}_i) \mathbf{e}_r, \quad (1)$$

$$\frac{d\mathbf{r}_i}{dt} = \mathbf{v}_i. \quad (2)$$

Here m_i is the ion mass, \mathbf{v}_i is the ion velocity, \mathbf{r}_i is the ion position, e is the ion charge, c is the speed of light, \mathbf{E} is the electric field, \mathbf{B} is the magnetic field, $g(\mathbf{r}_i)$ is the gravity from

the central object, and \mathbf{e}_r is an unit vector of r -component. Throughout this paper the vertical component (z -direction) of the gravity is ignored, and in the background rotation, balance between the gravity and the centrifugal force, $m_i g(\mathbf{r}_i) = m_i r \Omega_0^2$ is satisfied.

The electron, on the other hand is assumed to be a massless charge neutralizing fluid, and a generalized Ohm's law is given by

$$\mathbf{E} = -\frac{1}{c} \mathbf{v}_e \times \mathbf{B} + \frac{1}{n_e e} \nabla p_e + \eta \mathbf{J}, \quad (3)$$

where $n_e = n_i$ is the number density of the electrons (ions), \mathbf{v}_e is the moment averaged velocity of the electron, η is the resistivity and \mathbf{J} is the current density. Since we focus on the ion physics and assume the kinetic processes of the electrons, such as pitch angle scattering would take place much faster than those of the ions, we take the electron pressure, p_e as a scalar variable and assume to be given by an adiabatic relation,

$$p_e \propto n_e^\gamma, \quad (4)$$

where $\gamma = 5/3$ is the adiabatic constant. In addition, the Coriolis force, the centrifugal force and the gravity are neglected for the electrons because of a limit $m_e \rightarrow 0$. Finally, with the Maxwell equations under the Darwin approximation,

$$\nabla \cdot \mathbf{B} = 0, \quad (5)$$

$$\mathbf{J} = \mathbf{J}_e + \mathbf{J}_i = \frac{c}{4\pi} \nabla \times \mathbf{B}, \quad (6)$$

$$\frac{\partial \mathbf{B}}{\partial t} = -c \nabla \times \mathbf{E}, \quad (7)$$

we obtain a closed set of equations.

In this study we investigate the evolution of the system in the meridional plane (r, z), of the accretion disk. Since we focus on the localized region of the accretion disk, we approximate the background differential rotation with a linear profile. Introducing the following transformation,

$$x = r - r_0, \quad (8)$$

$$z = z, \quad (9)$$

and applying the tidal expansion on the Hill coordinate [Hill (1878)], the equation of motion (1) becomes,

$$m_i \frac{d\mathbf{v}_i}{dt} = e \left(\mathbf{E} + \frac{1}{c} \mathbf{v}_i \times \mathbf{B} \right) - 2m_i \boldsymbol{\Omega}_0 \times \mathbf{v}_i - 2m_i q \Omega_0^2 x \mathbf{e}_x, \quad (10)$$

where \mathbf{e}_x is an unit vector of x -component and $q = \partial \ln \Omega / \partial \ln r|_{r=r_0}$ and for a Keplerian rotation ($g(\mathbf{r}_i) \propto r^{-2}$), q is equal to $-3/2$. Note that as we assume the size of the simulation domain is much smaller compared to r_0 , the above equations may now be expressed in the Cartesian coordinate. Under this approximation, we can write the background Keplerian velocity in the corotating frame as,

$$\mathbf{v}_K = q \Omega_0 x \mathbf{e}_y, \quad (11)$$

where \mathbf{e}_y is an unit vector of y -component. Because of this background flow, non-zero electric field $\mathbf{E}_K = -\mathbf{v}_K \times \mathbf{B} / c$ is always observed in the corotating frame. Since this electric field is a function of x , charge neutrality is not exactly satisfied in this system. The magnitude of the charge inequality is estimated as,

$$\begin{aligned} \frac{\nabla \cdot \mathbf{E}_K}{n_{i0} e} &= -\frac{1}{n_{i0} e c} q \Omega_0 B - \frac{1}{n_{i0} e c} q \Omega_0 B \left. \frac{\partial \ln B}{\partial \ln x} \right|_{x=0} \\ &= -4\pi \frac{V_A^2}{c^2} \frac{\Omega_0}{\Omega_{ci}} \left(1 + \left. \frac{\partial \ln B}{\partial \ln x} \right|_{x=0} \right), \end{aligned} \quad (12)$$

where $V_A = B/\sqrt{4\pi n_{i0} m_i}$ is the Alfvén velocity and $\Omega_{ci} = eB/m_i c$ is the cyclotron frequency of the ions. In an usual accretion disk, $\Omega_0/\Omega_{ci} \ll 1$ holds and also under the hybrid framework $V_A/c \rightarrow 0$ is assumed. Therefore the inequality of the charge due to the differential rotation can be neglected in the hybrid framework. For the integration of equation (10) we use the ordinary Buneman-Boris method with transformed electric/magnetic field,

$$\mathbf{E}^* = \mathbf{E} - 2 \frac{m_i}{e} q \Omega_0^2 x \mathbf{e}_x, \quad (13)$$

$$\mathbf{B}^* = \mathbf{B} + 2 \frac{m_i c}{e} \Omega_0. \quad (14)$$

For update of \mathbf{E} and \mathbf{B} we adopt the iterative method proposed by Horowitz, Shumaker, and Anderson (1989).

B. Initial Conditions and Simulation method

As mentioned in the former section we investigate an evolution of the system in the 2.5 dimensional meridional (x, z) plane. The size of the domain is set to be $L_x \times L_z = 160 \times 960$ cells whose grid interval (Δx) is set to be the half of the ion inertia length (λ_i). As an initial condition we adopt double Harris sheets [Harris (1962)] along z -direction,

$$B_{z0}(x) = B_0 \left[\tanh\left(\frac{x - x_c(t)}{l}\right) - \tanh\left(\frac{x - x'_c(t)}{l}\right) - 1 \right]. \quad (15)$$

Here l is the width of the current sheet and is set to be $1.8\lambda_i$ throughout this article. $x_c(t), x'_c(t)$ is the center of each current sheet and as we shall discuss in Appendix B, the center of current sheet is not fixed in our simulation model. Initially $x_c(0)$ and $x'_c(0)$ are located on $L_x/4, 3L_x/4$, respectively. To satisfy the initial pressure equilibrium ($B^2/8\pi = n_c(T_i + T_e)$), ions are assumed to have a spacial distribution of,

$$n_i(x) = n_c \left[\cosh^{-2}\left(\frac{x - x_c(t)}{l}\right) + \cosh^{-2}\left(\frac{x - x'_c(t)}{l}\right) \right] + n_0, \quad (16)$$

where n_c is the number density at the center of the current sheet and n_0 is the number density in the outside of the current sheet region. In the following calculations we use 55 superparticles per cell in the outside of the current sheet region. For the velocity distribution the ions are assumed to have a shifted-Maxwellian distribution with a background Keplerian rotation,

$$f_i(\mathbf{x}_i, \mathbf{v}_i) = n_i(x) \left(\frac{m_i}{2\pi T_i}\right)^{3/2} \exp\left[-\frac{m_i}{2T_i} \left(v_x^2 + (v_y - v_{Ky}(x) - v_{d,i})^2 + v_z^2\right)\right], \quad (17)$$

where T_i is the initial temperature of the ion and $v_{d,i}$ is the ion drift velocity which is defined as,

$$v_{d,i} = 2 \frac{T_i}{B_0 l}. \quad (18)$$

In the following, all physical quantities are normalized with those of the parameters in the outside of the current sheet region. In the collisionless accretion disks such as disks around a black holes, the temperature of the electrons is considered to be much colder than that of the ions [Narayan, Yi, and Mahadevan (1995)]. Therefore we set the initial temperature of the electron as $T_e = 5 \times 10^{-3} T_i$. To save the integration time, we put localized perturbation in y -component of the vector potential following the form introduced in Zenitani *et al.* (2011),

$$\begin{aligned} \delta A_y = & 2lB_1 \exp\left[-\frac{(x - x_c(t))^2 + (z - z_X)^2}{(2l)^2}\right] \\ & - 2lB_1 \exp\left[-\frac{(x - x'_c(t))^2 + (z - z'_X)^2}{(2l)^2}\right], \end{aligned} \quad (19)$$

where $z_X = L_z/4$, $z'_X = 3L_z/4$ is the z -coordinate of the X-point and B_1 is the strength parameter of the perturbation which is set to be $0.12B_0$ in this calculation. In addition, we include a localized resistivity in the X-points,

$$\eta = \eta_0 + \eta_c \cosh^{-2} \left[\left(\frac{x - x_c(t)}{0.5\lambda_i} \right)^2 + \left(\frac{z - z_X}{\lambda_i} \right)^2 \right] + \eta_c \cosh^{-2} \left[\left(\frac{x - x'_c(t)}{0.5\lambda_i} \right)^2 + \left(\frac{z - z'_X}{\lambda_i} \right)^2 \right], \quad (20)$$

and the magnetic Reynolds numbers defined with $\lambda_i V_{A0}/\eta_0$ and $\lambda_i V_{A0}/\eta_c$ are set to be 2000 and 200, respectively. Here we impose the uniform resistivity since the magnetic reconnection does not occur in the ideal MHD limit. Therefore, we choose sufficiently small value of the resistivity for the uniform component and compare our results with the theory of the MRI under the ideal MHD approximation. The localized resistivity is imposed as anomalous resistivity due to the several instabilities generated in the vicinity of the X-point, such as lower hybrid instability [e.g. Higashimori and Hoshino (2012)]. As we will discuss in Appendix B, we have confirmed that the following results are not affected by the localized resistivity. With this initial condition we perform five runs varying the rotational parameter (Ω_0/Ω_{ci}). We choose RUN A which has no rotation as a fiducial run and gradually increase the rotational parameter. Several important parameters in the calculation are described in Table I. In RUN B and C the rotational parameter does not exceed the instability criteria for the MRI defined with the parameters in the outside of the current sheet region,

$$\Omega_0^2 > \frac{k^2 V_{A,Out}^2}{3}. \quad (21)$$

On the other hand with the rotational parameter used in RUN D and E, the entire domain is unstable to the MRI. In RUN D resulting fastest growing wavelength of the MRI defined with the parameters in the outside of the current sheet region is the same as L_z , whereas in RUN E the fastest growing wavelength is the same as $L_z/2$.

As we take the background differential rotation into account, the evolution of the MRI is recovered in this hybrid code with a uniform background plasma. In RUN F we impose uniform plasma to calculate a linear growth of the MRI. In high β_i plasma ($\beta_i \gtrsim 100$) rich kinetic effect of the ions such as generation of pressure anisotropy [Hoshino (2013)], and finite Larmor radius effect [Ferraro (2007)], would modify the linear behavior of MRI. However, since we simply aim to focus on the conventional evolution of MRI, we set $\beta_i = 1.0$ in this calculation. In this run we impose 800 superparticles per cell whose grid interval was set to be $\Delta x = \lambda_i$. In this run the size of the domain is set to be $L_x \times L_z = 80 \times 480$ and the rotational parameter is set to be the same as the one used in RUN E. Thus mode 2 of the MRI is expected to be the fastest growing mode in this calculation. The other parameters used in the simulation are listed in Table I.

TABLE I. Simulation Parameters.

	RUN A	RUN B	RUN C	RUN D	RUN E	RUN F
$L_x \times L_z$	160 × 960	160 × 960	160 × 960	160 × 960	160 × 960	80 × 480
λ_i	2 Δx	2 Δx	2 Δx	2 Δx	2 Δx	Δx
n_c/n_0	4	4	4	4	4	-
$\beta_{i,Out}$	1.0	1.0	1.0	1.0	1.0	1.0 ^a
p_e/p_i	5×10^{-3}	5×10^{-3}	5×10^{-3}	5×10^{-3}	5×10^{-3}	5.0×10^{-3}
Ω_0/Ω_{ci}	0	2×10^{-4}	5×10^{-3}	1.35×10^{-2}	2.70×10^{-2}	2.70×10^{-2}
Current Sheet ?	YES	YES	YES	YES	YES	NO

^a As we consider uniform plasma, $\beta_i = 1.0$ is assumed in the entire domain in this run.

III. RESULTS

A. Linear growth of MRI

First, we briefly look at the evolution of the MRI. Figure 1 shows the time evolution of the density and the magnetic field line in RUN F. As expected in the previous section, mode 2 of the MRI which can be clearly observed in Figure 1, is the most unstable with the parameters used here. As it is often reported in the MHD calculations, two sets of channel flows are generated in the final state of the calculation.

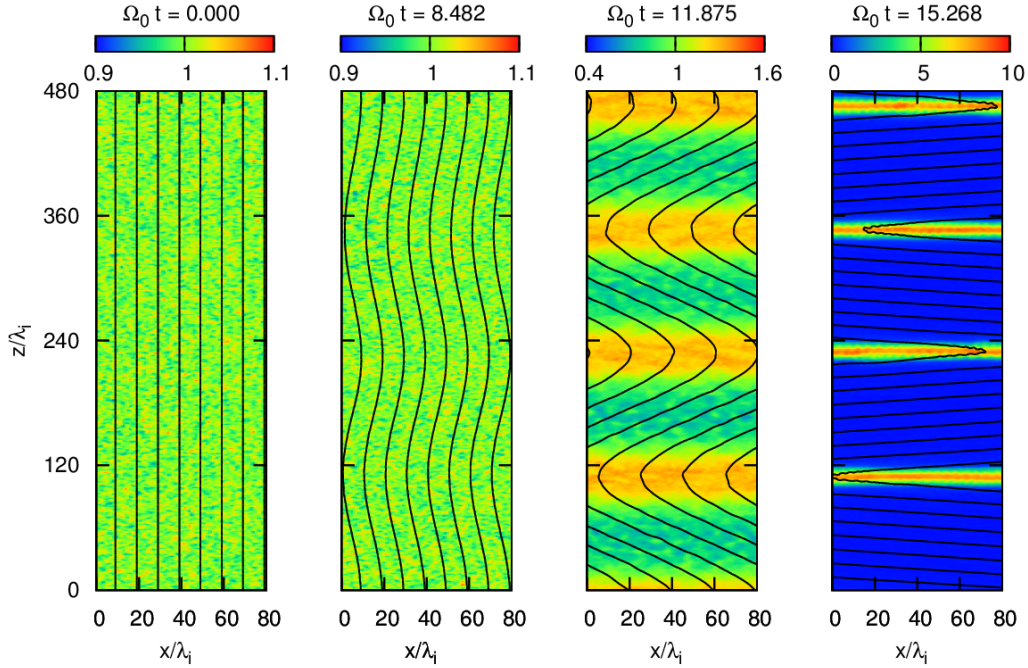


FIG. 1. Time evolution of the MRI. The color contour corresponds to the ion density and the solid line corresponds to the magnetic field line.

The linear growth of the MRI is also confirmed with the Fourier decomposition. In Figure 2 we show a growth rate obtained from our simulation. The horizontal axis corresponds to the normalized wavenumber whereas the vertical axis corresponds to the growth rate. Solid curve corresponds to a dispersion relation of the MRI obtained from the linear analysis of a Hall MHD equations [Balbus and Terquem (2001)], whereas the open circles correspond to the results from our hybrid simulation. As we can see from the plot, our results are in good agreement with those of the conventional MRI.

B. Magnetic Reconnection: Overview

Let us go on to the results of the magnetic reconnection. We first overview our results. Figure 3 shows the structures of five runs at the each stage of the reconnection. The most distinct feature is found in RUN E whose magnetic field line in the entire region of the simulation domain is remarkably bent. We consider that in this parameter the MRI is the dominant process for the evolution of the system. The relation between the magnetic reconnection and the MRI shall be discussed in the following section. In RUN B,C and D the effect of the Kepler rotation seems to be relatively moderate compared to RUN E. At the onset stage of the reconnection ($\Omega_{ci}t \simeq 144$) there is no significant difference in the

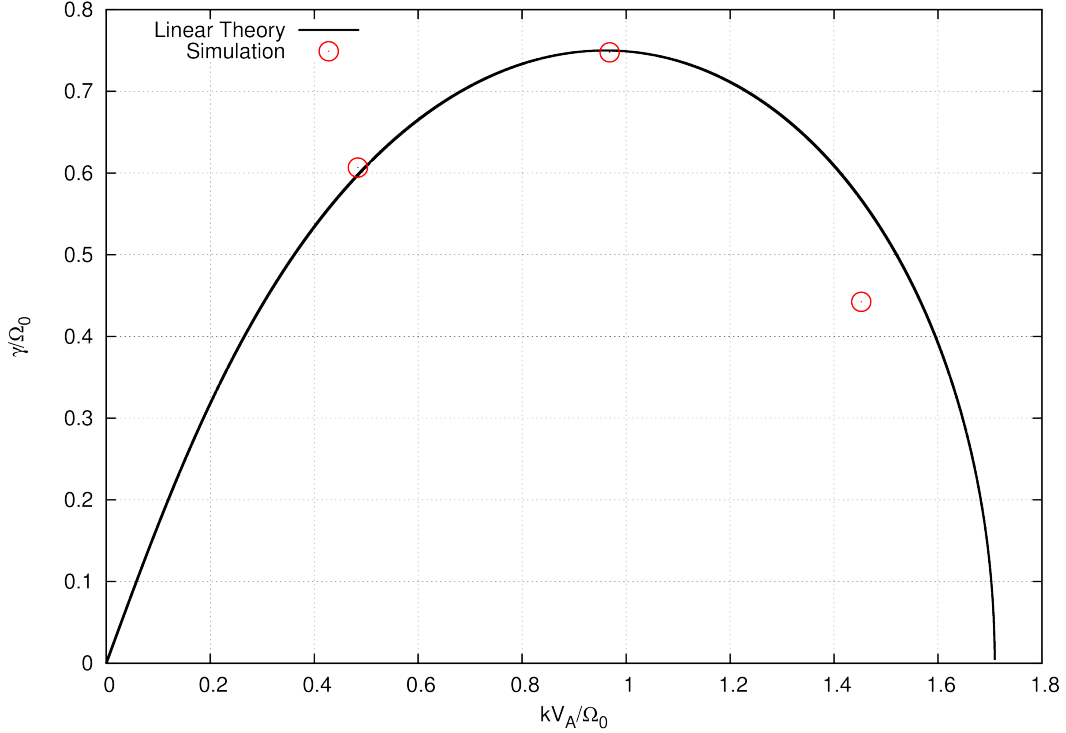


FIG. 2. The dispersion relation of the MRI. The open circles corresponds to a growth rate obtained from the simulation. Error bars are smaller than the size of the open circles.

structure between each run. However, as the reconnection goes on, an asymmetric structure gradually becomes remarkable in RUN B, C and D. The asymmetry becomes clearer as the rotational parameter increases. In addition, a migration of X-point is observed in all run with the finite Kepler rotation (RUN B-E). A physical interpretation of this migration shall also be discussed in the following section. Another asymmetry is also found in the out-of-plane magnetic field. Figure 4 shows the structure of the out-of-plane magnetic field (B_y) at the final stage of five runs. It is clear, especially in RUN C and D, the absolute value of B_y is, in average, larger in the right side of the X-point compared to that in the left side. This is understood by considering the coupling of the Hall effect and the differential rotation and shall be discussed in the next section.

C. Magnetic Reconnection: Asymmetric evolution of out-of-plane magnetic field

It is well known that the quadrupole structure in the out-of-plane magnetic field is observed around the X-point in the numerical simulation under the framework which distinguishes the magnetization degree of the ions and the electrons. In the hybrid framework which treats the ions as superparticles with finite mass and the electrons as massless charge neutralizing fluid, the magnetization feature of each component is also distinguished. This gives a significant difference in the motion of each component around the X-point resulting the in-plane Hall current and out-of-plane magnetic field [Sonnerup (1979)].

In our fiducial run (RUN A), a clear quadrupole structure is also found in the symmetric manner (Figure 4). As we pointed out in the previous section an asymmetric structure in the out-of-plane magnetic field (B_y) is found in RUN B, C and D. The asymmetry becomes significant as the rotational parameter increases. Figure 5 shows a focused view of the out-of-plane magnetic field (B_y) at $\Omega_{\text{ci}}t \simeq 437$ of RUN D. The color contour in the right panel

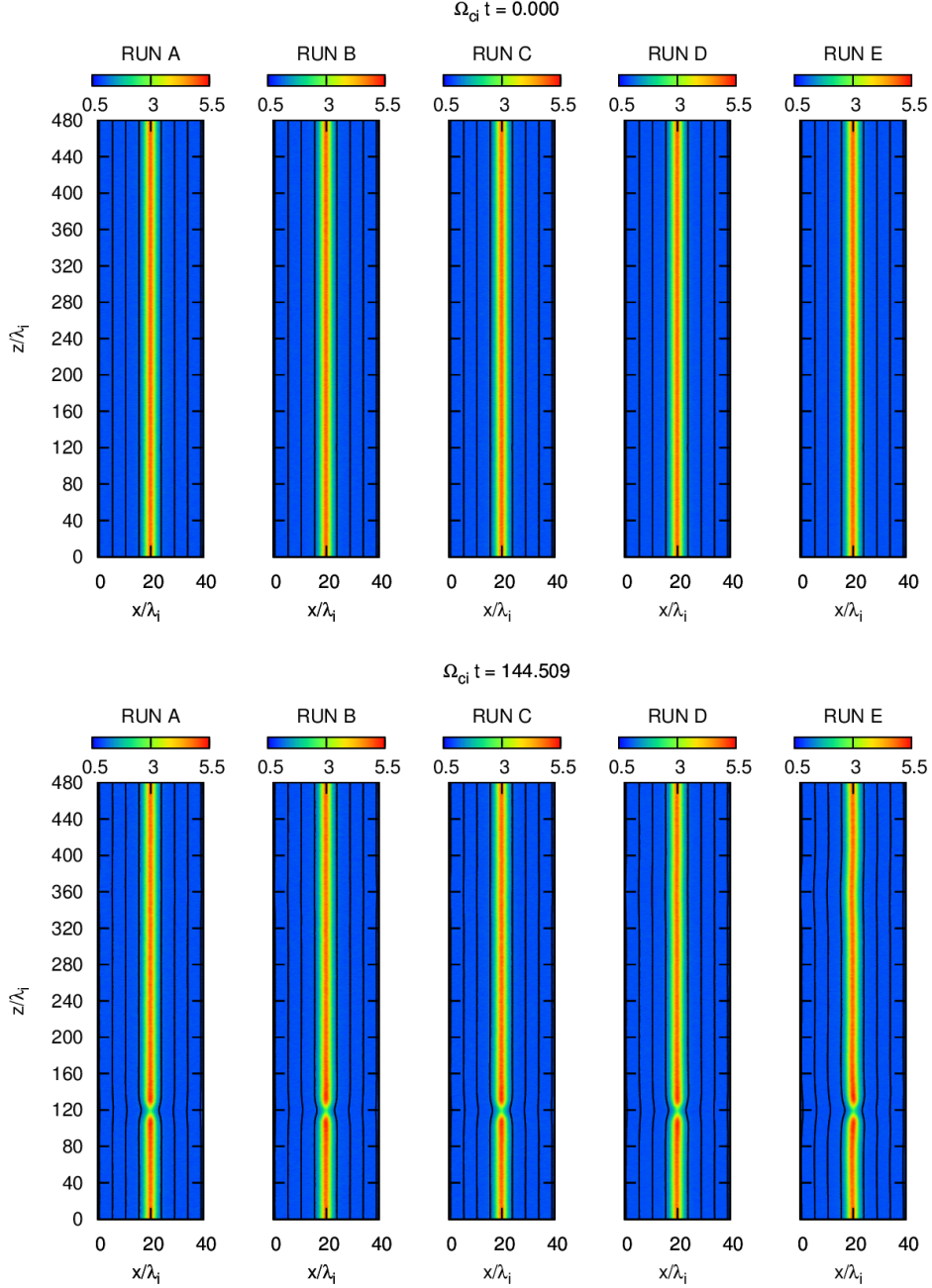


FIG. 3. The time evolution of all runs. The color contour corresponds to ion density whereas the solid line corresponds to the magnetic field line. The figures are focused on the left half of the simulation domain.

corresponds to B_y . In the left panel of Figure 5, B_y is also plotted along the dotted line denoted in the right panel, and from the top to the bottom each panel corresponds to line A-D. The dashed red lines plotted vertically in the left panels correspond to the baseline which passes through the X-point. In cut C and D clear asymmetry with respect to the red line is observed and the absolute value of B_y is always found to be large in the right side of the X-point compared to the left side. These structures can be understood by a simple coupling between the Hall magnetic field produced by the reconnection and the effect of the differential rotation.

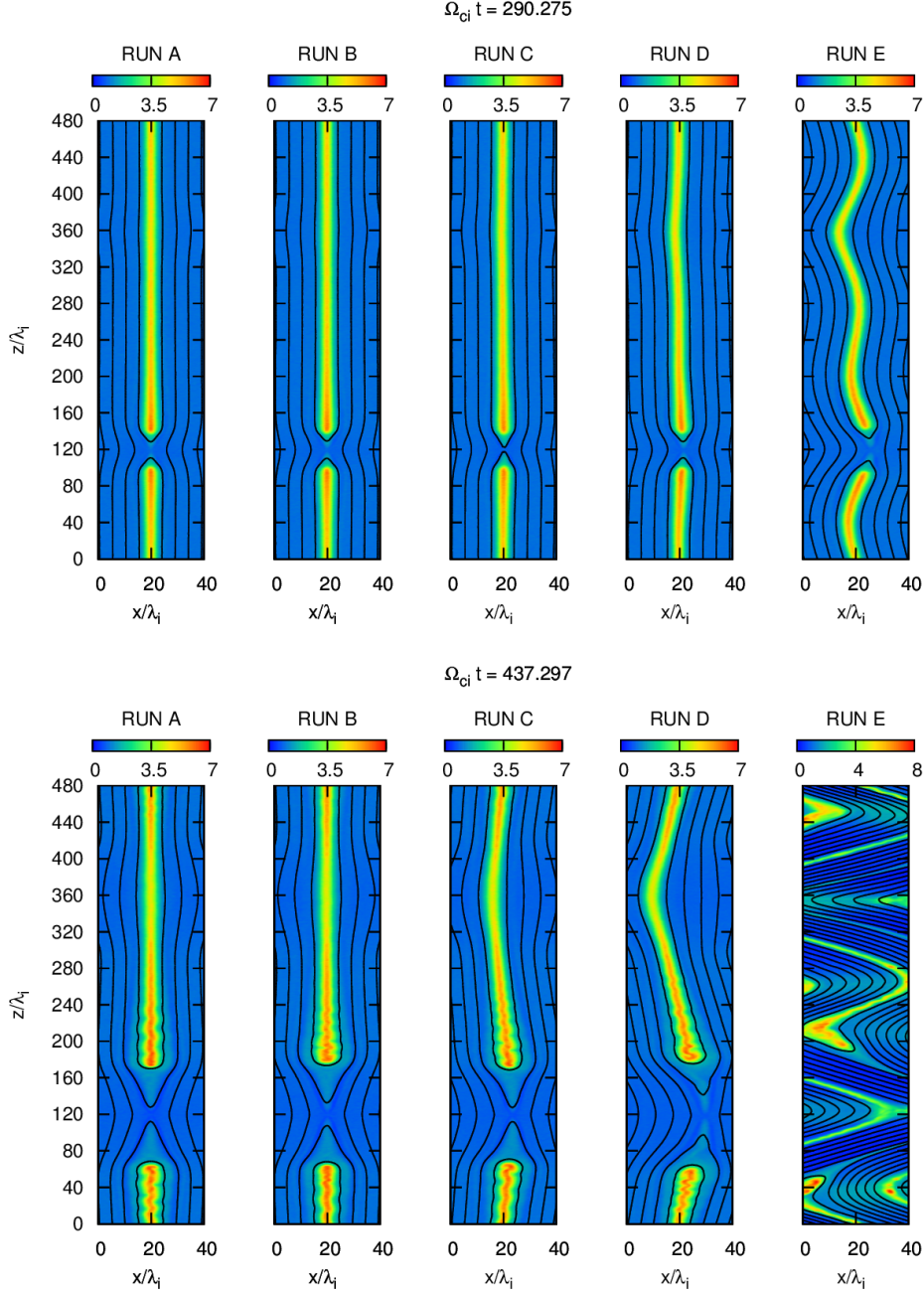


FIG. 3. Continued.

Figure 6 shows the schematic view of the system. As the reconnection grows the quadrupole magnetic field parallel to the y -axis is generated due to the Hall effect. As the reconnection goes on and B_x is generated the dynamo effect of the differential rotation produces B_y following to the y -component of the induction equation (A3). Since B_x generated by the reconnection has opposite sign on the different side of the X-point so as B_y generated by the shear motion. Superposing the quadrupole B_y due to the Hall current and the antisymmetric B_y due to the shear motion, the asymmetric structure in the out-of-plane magnetic field is clearly understood and in the case of Figure 6, for instance, the larger absolute value of B_y is observed in the right side of the X-point.

Paying attention to the fine structure, the “undulated” feature in the out-of-plane mag-

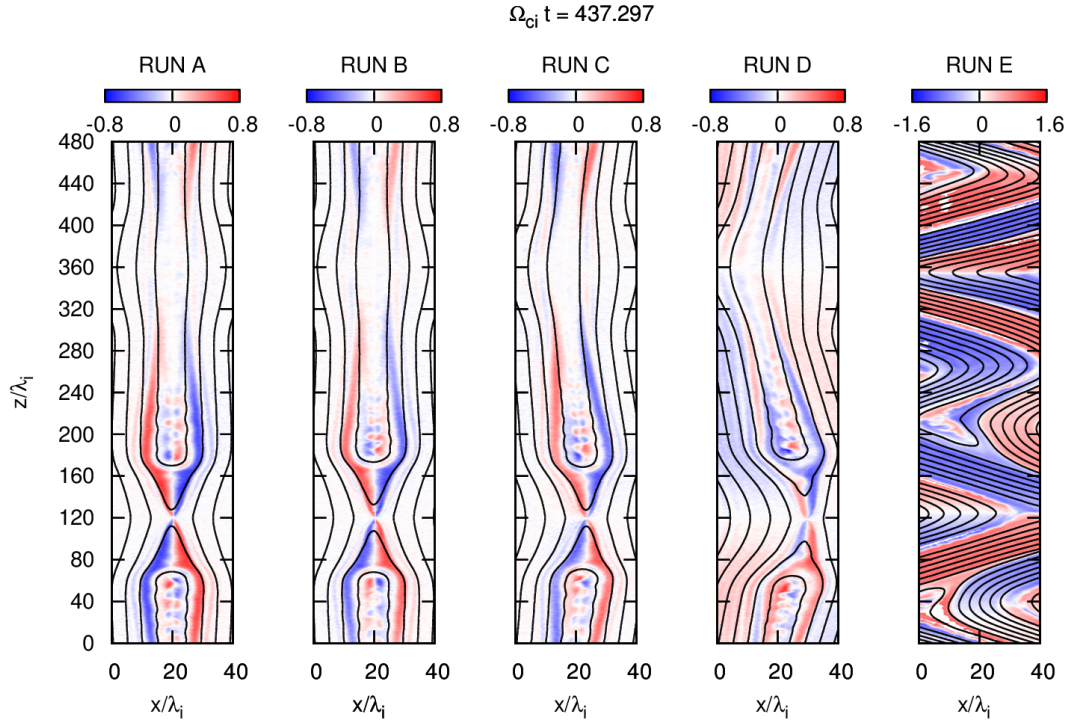


FIG. 4. The out-of-plane magnetic field (B_y) in the final stage of the simulation. B_y in RUN E is remarkably enhanced due to the dynamo effect of the MRI. The figures are focused on the left half of the simulation domain.

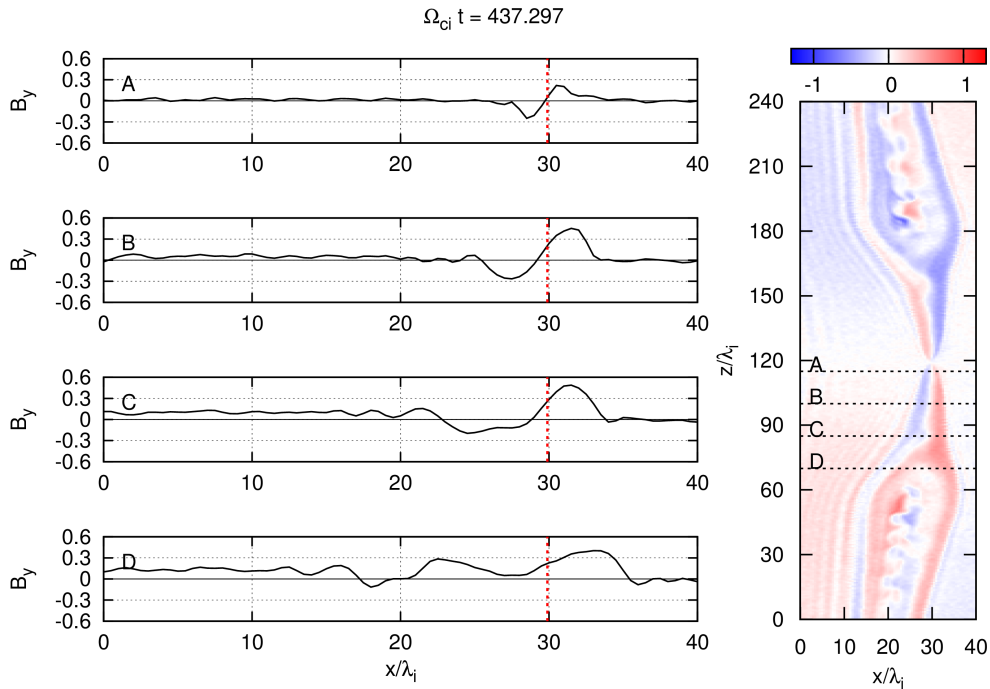


FIG. 5. Focused view of out-of-plane magnetic field in RUN D.

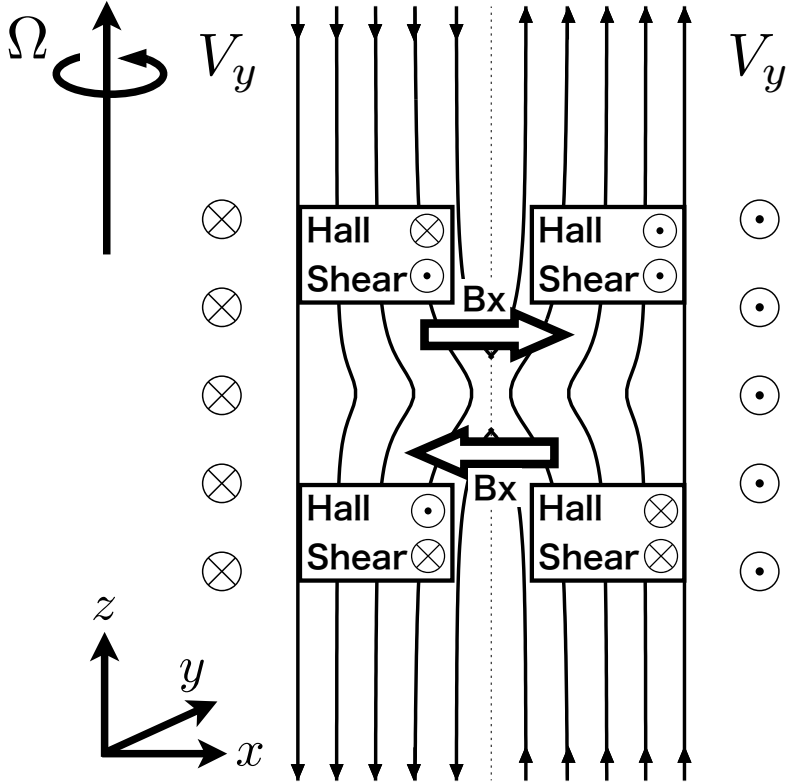


FIG. 6. A schematic plot of the Hall Field and the sheared Field.

netic field is found in the nonlinear stage of the reconnection. This structure is consistent with the one introduced in Arzner and Scholer (2001). They have pointed out that the structure is a consequence of an instability driven by a shear flow and a parallel pressure anisotropy generated in the layer consisted with the outflow region and the outside of the current sheet region. We note that in our simulation setup with the finite rotational parameters, any scale of perturbation would be unstable to the MRI inside the current sheet following to the conventional definition of the MRI criteria. This is because inside the current sheet the magnetic field gradually decreases whereas the density increases which leads to $V_{A,Out} \rightarrow 0$ in the right hand side of the equation (21). However as we can see from Figure 4, the characteristic scale of the “undulated” structure seems to be insensitive to the rotational parameter. Thus this structure can also be considered as the one introduced in Arzner and Scholer (2001) and the modulation by the MRI seems to be rather weak in this instability. In addition, a standing wave structure whose wave front is approximately parallel to the magnetic field line is found in the region where the transition takes place from the current sheet to the outside region. Approximating the structure of current sheet as a slow shock, this wave structure is regarded as a standing wave train found in the dispersive shock when the ion inertia scale is much larger than the resistive scale [Hau and Sonnerup (1992)]. These fine structures are found not only in RUN D but also in RUN A-C on which the effect of the Kepler rotation is relatively moderate.

D. Magnetic Reconnection: Migration of the X-points

Another remarkable structure is found in the vicinity of the X-point. As described in the overview the asymmetry becomes significant as time goes by. At the same time, the X-point

migrates in a certain direction. The direction of the X-point migration is always the same as long as the sign of $\mathbf{J}_0 \times \boldsymbol{\Omega}_0$, and we observe the migration in the opposite direction with the opposite sign of $\mathbf{J}_0 \times \boldsymbol{\Omega}_0$. The migration distance of the X-point is larger in the runs with the larger rotational parameter. Figure 7 shows a focused view of the X-point at $\Omega_{\text{ci}} t \simeq 437$ in RUN D. Here, the color contour in the right panel corresponds to the ion density. In the left panels, we show several physical values along the dashed white line indicated in the right panel. From the top, the density (solid line) and the pressure (dashed line) of the ions, the moment averaged ion velocity ($V_{x,\text{ions}}$), the y -component ion velocity deviation from the background Kepler rotation ($V_{y,\text{ions}}$), and the magnetic energy normalized with the initial value in the outside of the current sheet region, are plotted. The horizontal red dashed line plotted in the second row corresponds to the migration velocity of the X-point. In average, inflow speed of the ions from the both sides of the X-point are the same in the rest frame of the X-point.

The migration of the X-point itself is easily understood by the generation of the flow by the MRI. However the correlation between the sign of $\mathbf{J}_0 \times \boldsymbol{\Omega}_0$ and the direction of the migration is not obvious. This correlation can be understood by considering the asymmetric growth of MRI with respect to the neutral sheet. Since the conventional criteria of the MRI is given by Equation (21), the MRI is always active inside the current sheet where the magnetic field strength and the ambient Alfvén velocity are infinitesimally small. However, since we have carried out the calculations under hybrid framework, the effect of the Hall term should also be taken into account. As reported in Balbus and Terquem (2001), the Hall term extends the unstable region of the MRI to a shorter wavelength when the orientation of the magnetic field and the background rotational vector is anti-parallel, and vice versa. Following to their dispersion relation, the effect of Hall term is still minor in the outside of the current sheet region in our simulations. However, in the vicinity of the current sheet, the time scale of the cyclotron motion may reach to that of the Kepler rotation, and as a result the Hall term would be effective in this region. In Figure 7, the ambient magnetic field is anti-parallel to the rotational vector in the left side of the current sheet and the instability criteria is reduced in this region. Therefore the small scale perturbation triggered by the magnetic reconnection would couple to the MRI and can be enhanced in this side of the current sheet, resulting a migration of the X-point, whereas in the opposite side of the current sheet, the characteristic scale imposed by the magnetic reconnection does not satisfy the criteria of the MRI under the Hall effect. From the second and the third row, we find $V_{x,\text{ions}}/V_{y,\text{ions}} > 0$ in the left side of the X-point which is also satisfied during the growth stage of the MRI. We consider this phase relation is also consistent with the above explanation. In addition to the calculation introduced in the present article, we have also varied the number of the superparticles and the grid interval and confirmed that the above results were not affected by these parameters.

E. Magnetic Reconnection: Magnetic reconnection as a trigger of the MRI

As we have described in the overview, in the outside of the current sheet region of RUN E perpendicular magnetic field is remarkably enhanced which implies the dominant process in this parameter regime is the MRI. During the evolution of the MRI, a magnetic reconnection also takes place with the associating X-point migration giving additional growth of B_x together with the reconnection. In this section, we point out that the reconnection would also contribute to a relatively large initial perturbation on the growth of the MRI.

In order to evaluate the effect of the magnetic reconnection on the evolution of the MRI we perform another comparative calculation. Here we choose RUN E as a fiducial run and another run (RUN E2) is calculated without the initial trigger for the magnetic reconnection; by excluding the initial vector potential (19) and taking $\eta_c = 0$ in the resistivity (20). Note that we have left the uniform component of the resistivity η_0 . Therefore, under this initial condition, both a tearing mode instability and an MRI would take place. Here the fastest growing mode of the MRI in the outside of the current sheet region is $0.75\Omega_0 \simeq 0.02\Omega_{\text{ci}}$

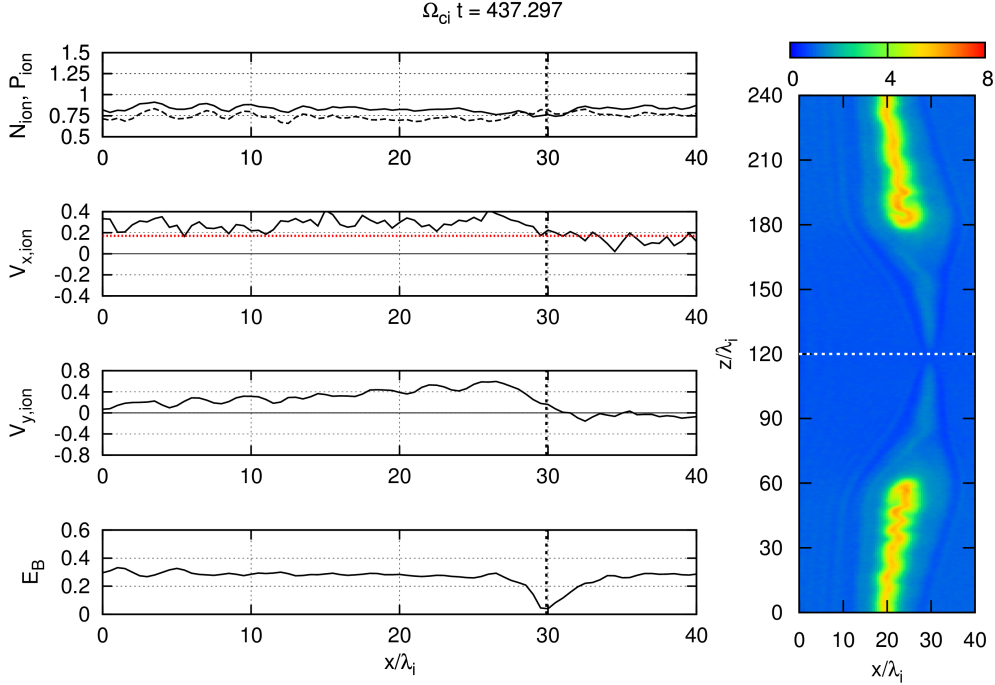


FIG. 7. A focused view of the X-point in RUN D.

which is comparable to that of a tearing mode which can roughly be estimated as $10^{-1}-10^{-2}\Omega_{ci}$ [e.g. Terasawa (1983); Hesse and Winske (1993)].

Figure 8 shows the time evolution of the two comparative runs. Again the color contour corresponds to the ion density, and the solid line corresponds to the magnetic field line. From the top panel ($\Omega_{ci}t \simeq 334$) we observe that the X-point in the different current sheet migrates in the opposite direction. From the bottom panel ($\Omega_{ci}t \simeq 437$) it is clearly observed that the perpendicular component of the magnetic field is significantly enhanced in RUN E.

Another distinct feature is also found from the Fourier decomposition of $|B_x|$ in each run. In Figure 9 we show the evolution curves of each mode in the both calculations. The Fourier transformation was applied on B_x along the z -axis in the outside of the current sheet region ($10\lambda_i \leq x \leq 20\lambda_i$). In this region, we can approximate the uniform plasma background and can compare results with the theory of conventional MRI. Within the two runs we find no significant difference in the maximum growth rate and was the same as that of the conventional MRI ($\gamma_{\max} = 0.75\Omega_0$) except for mode 3 in RUN E. During the initial growth stage of RUN E ($0\Omega_{ci}t - 100\Omega_{ci}t$) the growth rate is roughly $1.3\Omega_0$ which is about 1.8 times faster than that of the MRI. This implies that the magnetic reconnection and the associated X-point migration initially gives relatively large perturbation and act as an trigger for the MRI. During the middle stage of the evolution, the growth rates of all the modes do not exceed the maximum growth rate of the MRI. Triggered by the X-point migration, in this stage, the power of B_x in the outside of the current sheet region of RUN E is, in average, ~ 30 times larger than that of RUN E2. It is worth noting that the fastest growing mode in RUN E is mode 3 even the initial rotational parameter was set for mode 2 to be the most unstable. At the initial stage of reconnection, the reconnection rate corresponding to the separatrix angle determines the mode with the largest amplitude. At the same time, the X-point migration from the another current sheet gives perturbation towards opposite direction in $z \simeq 3L_z/4$. As a result at the initial growth stage a large amplitude perturbation corresponding to mode 3 is given by the magnetic reconnection and by the associating X-point migration. During the middle stage of the growth ($\Omega_{ci}t \gtrsim 100$) the ambient magnetic

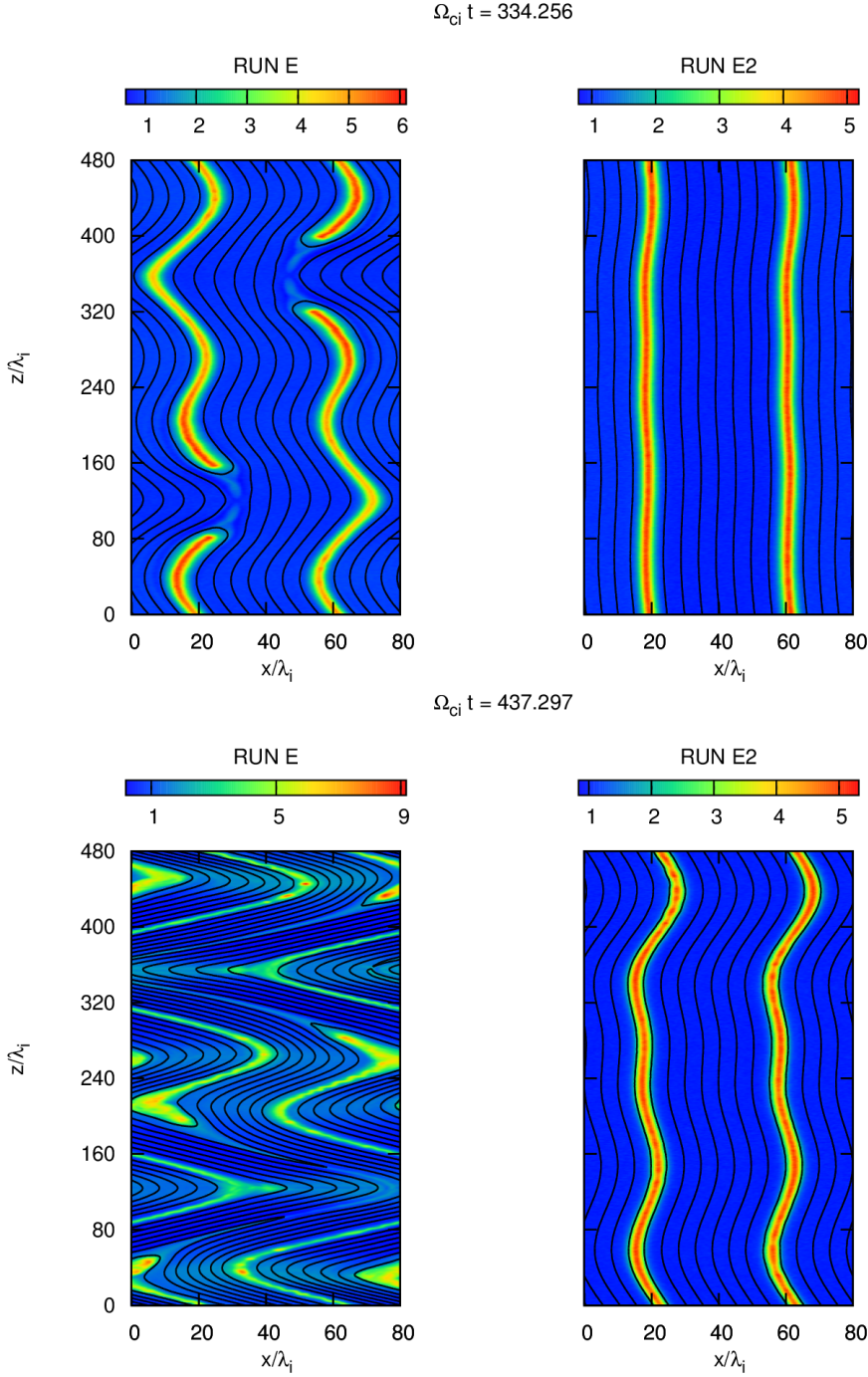


FIG. 8. The density (color) and the magnetic field line (solid line) at the middle stage of RUN E and RUN E2 (top), and at the final stage (bottom).

field parallel to the rotational axis is weakened by magnetic reconnection leading shorter wavelength to be more unstable to the MRI. It is well known that the linear process of a 2.5D MRI also holds even the perturbed field amplitude is relatively large compared to the ambient field [Goodman and Xu (1994)]. Therefore, in the middle stage of the evolution, mode 3 can be the most unstable.

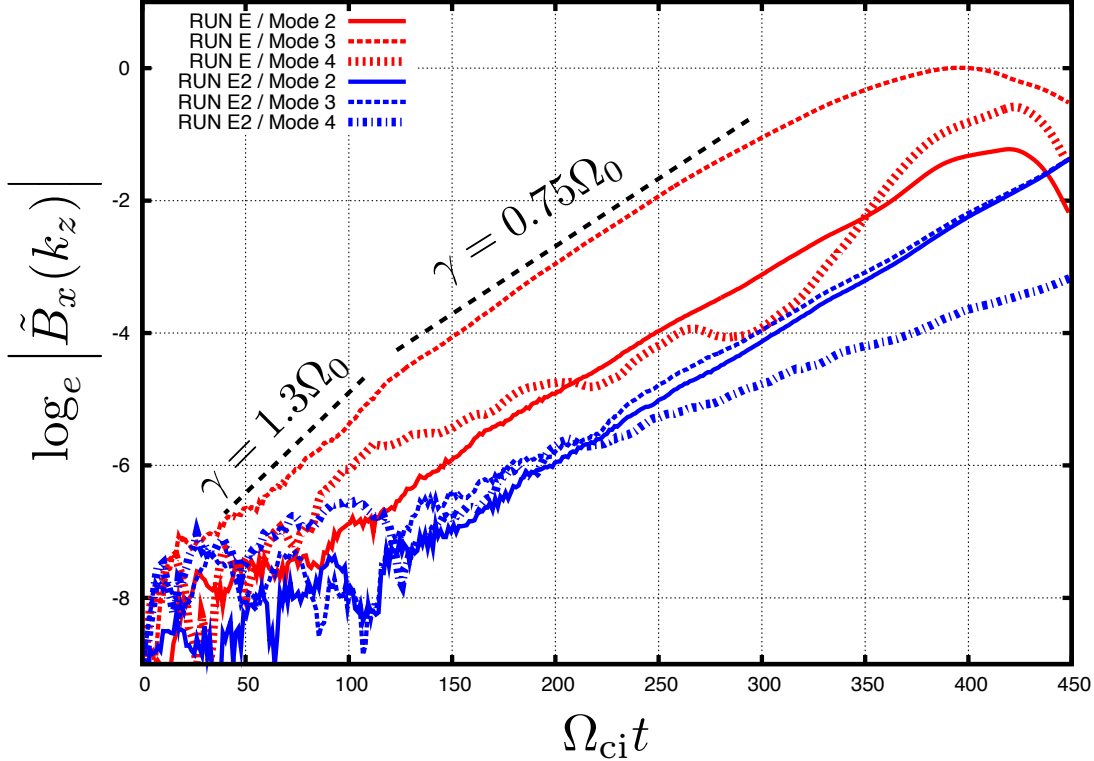


FIG. 9. The time evolution of Magnetic Field Power.

IV. SUMMARY AND DISCUSSIONS

In this study we developed a 2.5D hybrid code including the Coriolis and the tidal force which can be found in a local corotating frame with a standard open shearing boundary condition [Hawley, Gammie, and Balbus (1995)]. In this code, azimuthal symmetry is assumed and as a result, the boundary condition degenerates to a standard periodic boundary condition for the deviation components. With this code we first confirmed the evolution of the MRI. As a first step we focused on the linear growth of the instability in the low β_i limit so that we would neglect rich kinetic effects introduced in Hoshino (2013) and Ferraro (2007) and would compare the results with the conventional linear theory. The result was in good agreement with the conventional theory of the MRI. We note that the studies of long term evolution of MRI in the high β_i regime would be important to understand the relaxation process of the pressure anisotropy in the collisionless accretion disks.

We also investigated the effect of the differential rotation on the evolution of the magnetic reconnection with five consecutive runs. Main results are summarized as follows:

First we found an asymmetric structure in the out-of-plane magnetic field in the vicinity of the X-point. This can be understood by the coupling of the Hall term and the differential rotation. As the reconnection grows, a Hall current around the X-point generates quadrupole magnetic field. At the same time, the perpendicular magnetic field generated by the magnetic reconnection is sheared by the differential rotation generating a dipole structure in the out-of-plane magnetic field. The asymmetry is created as a superposition of these two processes. Furthermore, we also confirmed the “undulated” structure reported in Arzner and Scholer (2001). Here, the differential rotation seems to have a minor effect on the generation of the “undulated” structure.

Next we found a migration of the X-point. This can be interpreted as a result of the MRI evolution coupled with the magnetic reconnection under the Hall effect. Since we have

taken the Hall effect into account, the instability criteria of the MRI is different between the opposite sides of the neutral sheet. The particular side of the outside of the current sheet region has a reduced criteria of the MRI, whereas the another one has a severer criteria. Since a small scale perturbation given by the magnetic reconnection would couple with the MRI under the Hall effect in the particular side of the current sheet, the perturbation imposed by the magnetic reconnection would be enhanced in an asymmetric manner. This asymmetry in a growth of the MRI would result the migration of the X-point and its direction is determined only by the initial sign of $\mathbf{J}_0 \times \boldsymbol{\Omega}_0$.

Finally we found that the migration of the X-point can be a trigger of the MRI and can modify the characteristic scale of the perturbation. As the X-point migration generates relatively large B_x perturbation, the magnetic reconnection in the differentially rotating system can be an effective trigger of the MRI. At the same time, the magnetic reconnection annihilates the ambient magnetic field shifting the most unstable wavelength of the MRI to the smaller scale.

It is well known that during the quasi steady state of the MRI induced turbulence, the magnetic energy is enhanced intermittently and released within a short time scale. During this stage a disruption and a re-organization of the channel flow take place repeatedly and a magnetic reconnection plays an important role on the dissipation of the magnetic field and heating of plasma. This process generates spike structures in the time evolution of the Maxwell stress curve during the quasi steady state [Sano and Inutsuka (2001)]. It has also been pointed out from 2.5D PIC simulations that during the “active” phase when the magnetic reconnection takes place repeatedly the efficiency of the angular momentum transport increases [Hoshino (2013)]. These results imply that the repeating process of magnetic energy enhancement by the MRI and dissipation by the magnetic reconnection is essential to an effective angular momentum transport. Though our initial setting is limited in the specific structure of the current sheet, we consider that the “triggering” effect of magnetic reconnection would be an effective seed of a re-organization of the current sheet associated to the channel flow and as a result, contributes to a strong angular momentum transport in the collisionless accretion disk.

It is worth noting by using the hybrid code, we have bridged the scale gap between the MHD scale and the PIC scale. Though several hundreds of ion inertia scale is still be smaller than the actual scale of the disk, we believe that the results of the present article would be non-negligible in the thick current sheet. For fully understanding the evolution of the MRI, the associated generation and relaxation of pressure anisotropy, the dissipation by magnetic reconnection, and the resulting efficient angular momentum transport, a massive 3D simulation would be required. We would also like to point out that not only the 2.5D meridional plane analysis but also the equatorial (x, y) plane analysis would be important for the understanding of the fundamental physics of the magnetic reconnection in the differentially rotating system.

The author would like to acknowledge T.Amano, K.Higashimori, and K.Hirabayashi for valuable and insightful discussions. This research is supported in part by Grant-in-Aid for Japan Society for the Promotion of Science (JSPS) Fellows (No.10J08225), and JSPS Kakenhi (No.25287151).

Appendix A: Methods for calculating differentially rotating system using hybrid code.

Here we briefly describe about the modification applied in our hybrid code due to the differential rotation.

As we explained in Sec. II, we assume that the background Kepler rotation always exists. Therefore one must pay attention to the boundary condition since the out-of-plane flow velocity differs between the inner and outer boundary of the domain. However, as a Keplerian velocity can be exactly calculated from equation (11) we simply focus on the deviation from the Keplerian profile. Since we assume the azimuthal symmetry ($\partial/\partial y = 0$)

the open shearing boundary condition proposed by Hawley, Gammie, and Balbus (1995) degenerates to a standard periodic boundary condition for the deviation components.

For updating of the particles, we use the Buneman-Boris method. Here we use the particle velocity observed in the corotating frame; that is, all the particle velocity includes the Keplerian component in the time integration of the particle. At each time step we subtract the Keplerian velocity component of the particles using updated position information ($\mathbf{x}_i^{n+1/2}$). Then we apply a moment calculation to obtain the deviation component of the current density using an appropriate shape function,

$$\mathbf{J}_{i,\text{dev}}^{n+1/2} = e \sum_{\text{particle}} \mathbf{v}_{i,\text{dev}}^{n+1/2} S(\mathbf{x}_i^{n+1/2}). \quad (\text{A1})$$

From $\mathbf{J}_{i,\text{dev}}^{n+1/2}$ we calculate the deviation component of the electric field ($\mathbf{E}_{\text{dev}}^{n+1/2}$) by using the Ohm's law (3), and the Ampère's law (6). Note that since the simulation is performed under nonrelativistic limit, the magnetic field is Lorentz invariant. The electric field observed in the corotating frame is obtained by applying a Lorentz transformation on this electric field. This is applied by adding the induction term due to the Keplerian flow to the deviation component,

$$\mathbf{E}^{n+1/2} = \mathbf{E}_{\text{dev}}^{n+1/2} - \frac{1}{c} \mathbf{v}_K \times \mathbf{B}^{n+1/2}. \quad (\text{A2})$$

For the update of the magnetic field, we separate the $\nabla \times$ calculation of the electric field to the deviation component and the Keplerian component. As we assume the azimuthal symmetry ($\partial/\partial y = 0$), together with the solenoidal condition (5), the Keplerian component of the induction term is calculated as follows,

$$\frac{1}{c} \nabla \times (\mathbf{v}_K \times \mathbf{B}^{n+1/2}) = -\frac{1}{c} q \Omega_0 B_x^{n+1/2} \mathbf{e}_y. \quad (\text{A3})$$

This equation physically describes the shearing effect of the differential rotation generating the y -component magnetic field from the x -component. $\mathbf{B}^{n+1/2}$ and $\mathbf{E}^{n+1/2}$ are iteratively calculated in the update of the field. Since the periodicity is guaranteed for the deviation components and for the magnetic field, this separation of the $\nabla \times$ calculation greatly reduces the complication in taking the boundary condition with the shear flow.

Appendix B: Harris solution in differentially rotating system

Here we discuss the behavior of a Harris solution in the rotating system. A conventional Harris solution cannot be an exact kinetic equilibrium solution in a differentially rotating disk because the solution introduced in Harris (1962) is based on the conservation of the canonical angular momentum for each particle. In a differentially rotating disk the angular momentum due to the central massive object must be taken into account together with the angular momentum due to the cyclotron motion.

Considering the differential rotation under the Hill coordinate [Hill (1878)] we obtain a second order ordinary differential equation which degenerates to the one introduced in the equation (16) of Harris (1962) in the limit of $\Omega_0 \rightarrow 0$. The solution cannot be expressed with a superposition of simple functions. Therefore we have simply adopted a superposition of a conventional Harris solution and a Keplerian differential rotation as an initial asymptotic solution. Here we investigate whether this approximation is valid or not in the case of $\Omega_0/\Omega_{ci} \ll 1$. We carry out five comparative runs with no initial trigger for the magnetic reconnection, i.e. $B_1 = 0$ in Equation (19) and $\eta_c = 0$ in Equation (20), with the rotational parameter used in the main runs. We also restrict the vertical size of the simulation domain (L_z) to guarantee the outside of the current sheet region to be stable to the MRI. From the results, it is confirmed that the initial structure of the current sheet is conserved in time. However, we also find that the neutral point of the current sheet moves in time.

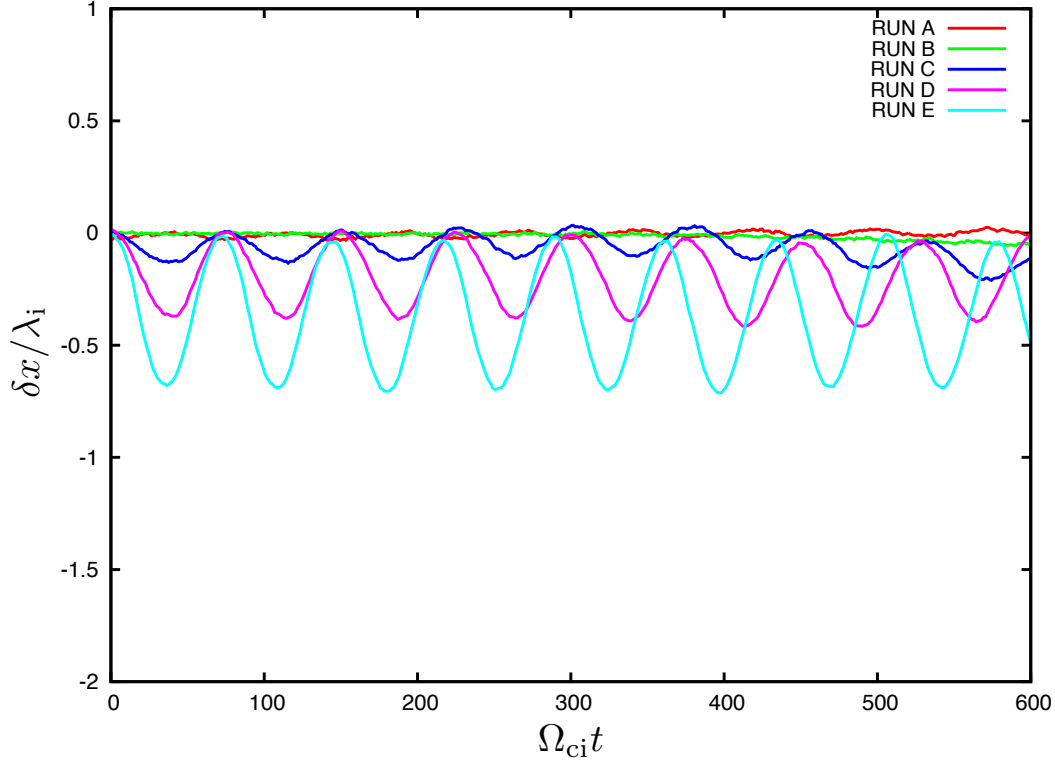


FIG. 10. The oscillation of the neutral point. The deviation from the initial neutral point (δx) in the unit of inertia length is plotted in the vertical direction.

Figure 10 shows the position of the neutral point observed in each calculation. As the rotational parameter increases the amplitude of oscillation becomes significant though its amplitude is smaller than the initial width of the current sheet. This is due to the initial current in the neutral sheet. Since in this calculation, the ions are hotter than the electrons, the dominant component with subject to an out-of-plane initial current is the ions. As the ions have finite mass in the hybrid framework, any initial motion inside the equatorial plane will couple to the differential rotation through the Coriolis force. In this case the initial out of plane drift $\pm V_y$ creates $\mp V_x$ with $\pi/2$ phase delays due to the Coriolis force. Once V_x has created the compression and the expansion of the plasma and the magnetic field take place since the direction of the drift motion is opposite with the each current sheet. Therefore, the oscillation can roughly be regarded as a perpendicular mode of the fast mode magnetosonic wave. The estimated frequency of perpendicular fast mode wave in this system is approximately $0.1\Omega_{ci}$, which roughly explains the results.

As the amplitude of this oscillation is relatively small throughout all the parameters used in this calculation we find it is valid to use a Harris solution as an approximate equilibrium solution in this system provided that the rotational parameter Ω_0/Ω_{ci} is sufficiently small. However, since the anomalous resistivity is imposed locally in the current sheet center, and since the current sheet oscillates in time, one must pay attention to the detection of the current sheet center. At each time step the current sheet centers ($x_c(t)$ and $x'_c(t)$) are detected by calculating a local maximum of $|(\nabla \times \mathbf{B})_y|$ in the vicinity of the current sheet centers which has also been detected in the previous time step.

It is worth noting that the initial direction of V_x generated by the neutral sheet current and the direction of the X-point migration introduced in Sec. III is opposite. In addition, we have also confirmed, by setting $\eta_c = 0$ in equation (20), that the way of detecting the

current sheet center does not affect the direction of the X-point migration. Therefore, we conclude that the X-point migration is independent to an initial plasma sheet oscillation and purely a result of coupling with the structure of the reconnection and the differential rotation.

- Arzner, K. and Scholer, M., “Kinetic structure of the post plasmoid plasma sheet during magnetotail reconnection,” *Journal of Geophysical Research* **106**, 3827–3844 (2001)
- Asano, Y., Mukai, T., Hoshino, M., Saito, Y., Hayakawa, H., and Nagai, T., “Evolution of the thin current sheet in a substorm observed by Geotail,” *Journal of Geophysical Research* **108**, 1189 (2003)
- Balbus, S. A. and Hawley, J. F., “A powerful local shear instability in weakly magnetized disks. I - Linear analysis. II - Nonlinear evolution,” *Astrophys.J* **376**, 214–233 (1991)
- Balbus, S. A. and Hawley, J. F., “Instability, turbulence, and enhanced transport in accretion disks,” *Reviews of Modern Physics* **70**, 1–53 (1998)
- Balbus, S. A. and Terquem, C., “Linear Analysis of the Hall Effect in Protostellar Disks,” *Astrophys.J* **552**, 235–247 (2001)
- Chandrasekhar, S., “The Stability of Non-Dissipative Couette Flow in Hydromagnetics,” *Proceedings of the National Academy of Science* **46**, 253–257 (1960)
- Chew, G. F., Goldberger, M. L., and Low, F. E., “The Boltzmann Equation and the One-Fluid Hydro-magnetic Equations in the Absence of Particle Collisions,” *Royal Society of London Proceedings Series A* **236**, 112–118 (1956)
- Ferraro, N. M., “Finite Larmor Radius Effects on the Magnetorotational Instability,” *Astrophys.J* **662**, 512–516 (2007)
- Goodman, J. and Xu, G., “Parasitic instabilities in magnetized, differentially rotating disks,” *Astrophys.J* **432**, 213–223 (1994)
- Harris, E. G., “On a plasma sheath separating regions of oppositely directed magnetic field,” *Il Nuovo Cimento* **23**, 115–121 (1962)
- Hau, L.-N. and Sonnerup, B. U. O., “The thickness of resistive-dispersive shocks,” *Journal of Geophysical Research* **97**, 8269–8275 (1992)
- Hawley, J. F. and Balbus, S. A., “A Powerful Local Shear Instability in Weakly Magnetized Disks. II. Nonlinear Evolution,” *Astrophys.J* **376**, 223 (1991)
- Hawley, J. F. and Balbus, S. A., “A powerful local shear instability in weakly magnetized disks. III - Long-term evolution in a shearing sheet,” *Astrophys.J* **400**, 595–609 (1992)
- Hawley, J. F., Gammie, C. F., and Balbus, S. A., “Local Three-dimensional Magnetohydrodynamic Simulations of Accretion Disks,” *Astrophys.J* **440**, 742 (1995)
- Hesse, M. and Winske, D., “Hybrid simulations of collisionless ion tearing,” *Geophysical Research Letters* **20**, 1207–1210 (1993)
- Higashimori, K. and Hoshino, M., “The relation between ion temperature anisotropy and formation of slow shocks in collisionless magnetic reconnection,” *Journal of Geophysical Research (Space Physics)* **117**, A01220 (2012)
- Hill, G. W., “Researches in the lunar theory,” *American Journal of Mathematics* **1**, pp. 5–26 (1878)
- Horowitz, E. J., Shumaker, D. E., and Anderson, D. V., “Qn3d: A three-dimensional quasi-neutral hybrid particle-in-cell code with applications to the tilt mode instability in field reversed configurations,” *Journal of Computational Physics* **84**, 279 – 310 (1989)
- Hoshino, M., “Particle acceleration during magnetorotational instability in a collisionless accretion disk,” *Astrophys.J* **773**, 118 (2013)
- Kulsrud, R. M., “MHD description of plasma,” in *Basic Plasma Physics: Selected Chapters, Handbook of Plasma Physics, Volume 1*, edited by A. A. Galeev and R. N. Sudan (1983) (Amsterdam: North-Holland) p. 1
- Matsumoto, R. and Tajima, T., “Magnetic viscosity by localized shear flow instability in magnetized accretion disks,” *Astrophys.J* **445**, 767–779 (1995)
- Narayan, R., Yi, I., and Mahadevan, R., “Explaining the spectrum of Sagittarius A* with a model of an accreting black hole,” *Nature* **374**, 623–625 (1995)
- Quataert, E., Dorland, W., and Hammett, G. W., “The Magnetorotational Instability in a Collisionless Plasma,” *Astrophys.J* **577**, 524–533 (2002)
- Riquelme, M. A., Quataert, E., Sharma, P., and Spitkovsky, A., “Local Two-dimensional Particle-in-cell Simulations of the Collisionless Magnetorotational Instability,” *Astrophys.J* **755**, 50 (2012)
- Sano, T. and Inutsuka, S.-I., “Saturation and Thermalization of the Magnetorotational Instability: Recurrent Channel Flows and Reconnections,” *Astrophys. J. Let.* **561**, L179–L182 (2001)
- Sano, T. and Stone, J. M., “The Effect of the Hall Term on the Nonlinear Evolution of the Magnetorotational Instability. I. Local Axisymmetric Simulations,” *Astrophys.J* **570**, 314–328 (2002)
- Shakura, N. I. and Sunyaev, R. A., “Black holes in binary systems. Observational appearance.” *Astron. & Astrophys.* **24**, 337–355 (1973)
- Sharma, P., Hammett, G. W., Quataert, E., and Stone, J. M., “Shearing Box Simulations of the MRI in a Collisionless Plasma,” *Astrophys.J* **637**, 952–967 (2006)
- Snyder, P. B., Hammett, G. W., and Dorland, W., “Landau fluid models of collisionless magnetohydrodynamics,” *Physics of Plasmas* **4**, 3974–3985 (1997)

- Sonnerup, B. U. Ö., “Magnetic field reconnection,” in *Solar System Plasma Physics*, edited by L. J. Lanzerotti, C. F. Kennel, and E. N. Parker (1979) (Amsterdam: North-Holland) pp. 45–108
- Terasawa, T., “Hall current effect on tearing mode instability,” *Geophysical Research Letters* **10**, 475–478 (1983)
- Velikhov, E., “Stability of an ideally conducting liquid flowing between rotating cylinders in a magnetic field,” *Journal Name: Zhur. Eksptl. i Teoret. Fiz.* **36**, 1398 (1959)
- Zenitani, S., Hesse, M., Klimas, A., Black, C., and Kuznetsova, M., “The inner structure of collisionless magnetic reconnection: The electron-frame dissipation measure and Hall fields,” *Physics of Plasmas* **18**, 122108 (2011)